Surface & Coatings Technology 214 (2013) 91–96

Contents lists available at SciVerse ScienceDirect

Surface & Coatings Technology

journal homepage: www.elsevier.com/locate/surfcoat

Structure and property of epitaxial titanium oxynitride grown on MgO(001) substrate by pulsed laser deposition

Hien Do [a,*], Yue-Han Wu [a], Van-Truong Dai [b], Chun-Yen Peng [a], Tzu-Chun Yen [a], Li Chang [a]

[a] Department of Materials Science and Engineering, National Chiao Tung University, Hsinchu, Taiwan 300, ROC
[b] Department of Electronics Engineering, National Chiao Tung University, Hsinchu, Taiwan 300, ROC

ARTICLE INFO

Article history:
Received 18 July 2012
Accepted in revised form 3 November 2012
Available online 16 November 2012

Keywords:
Titanium oxynitride
Epitaxial growth
Pulsed laser deposition
Nanoindentation

ABSTRACT

High-quality epitaxial TiN_xO_y films with different oxygen content were deposited on MgO(001) substrates by pulsed laser deposition method. The chemical composition of the deposited films was determined by X-ray photoelectron spectroscopy. X-ray diffraction results showed that the TiN_xO_y films are heteroepitaxially grown on MgO with good crystallinity and their lattice parameters decrease with increased oxygen concentration. Transmission electron microscopy analyses showed that TiNO films contain a low density of dislocations. Atomic force microscopy revealed very smooth surfaces of TiN_xO_y films with roughness of 0.26–0.29 nm. The resistivity of TiN_xO_y films determined by Hall measurement was about 28–33 μΩ cm. Nanoindentation measurements showed the film hardness and Young's modulus of about 23–26 GPa and 400–430 GPa, respectively.

© 2012 Elsevier B.V. All rights reserved.

1. Introduction

Titanium nitride (TiN) belongs to the family of refractory transition metal nitrides and possesses excellent optical, chemical, and physical properties that lead to many applications such as hard coating material, hard mask, and diffusion barriers [1–6]. The addition of oxygen to TiN matrix to form a new composition, i.e., titanium oxynitride (TiN_xO_y), has recently attracted attention. This is due to the fact that titanium oxynitride benefits from many remarkable properties of both metallic oxides (chemical stability, optical properties) and nitrides (hardness, wear resistance). Moreover, the optical and electrical properties of TiN_xO_y can be tailored between those of metallic nitrides and those of corresponding ionic oxides by varying the oxygen/nitrogen ratio [7,8]. Therefore, titanium oxynitride has been widely used in a wide range of applications such as decorative and wear-resistant coating [7,8], transparent IR window electrodes [7], solar collector devices [7,9], electrical switchable windows [10], and photocatalysis [11]. In comparison with TiN, titanium oxynitride has shown new interesting properties that can be used as biomaterials [12,13], memory devices [14]. In addition, titanium oxynitride nanocrystals with NaCl (rock-salt) structure especially show ultraviolet light emission in photoluminescence spectra at room temperature contrasted with the TiN case [15]. Another attractive motivation to study TiN_xO_y is that the presence of oxygen in the TiN films has beneficial effects on diffusion barrier performance for Al, e.g., the possibility of reducing the grain boundary diffusion and decreasing the contact failure rate during high temperature cycling [16–20].

TiN_xO_y films have been deposited by various processes, including the oxidation of TiN [21], nitridation of TiO_2 [22], and simultaneous mixing of elements or precursors methods such as magnetron sputtering [8], evaporation [9], metal organic chemical vapor deposition (MOCVD) [23], and pulsed laser deposition (PLD) [24]. In most cases, however, titanium oxynitride films have been reported to be amorphous or polycrystalline. Epitaxial growth of TiN_xO_y has been rarely studied in contrast with the case of TiN. The deposition of epitaxial TiN_xO_y can improve electrical conductivity and overcome the problem of fast grain boundary diffusion of dopants and impurities along the columnar grains of the polycrystalline films [18–20,25]. Furthermore, the study of epitaxial films can improve our understanding of the basic properties of TiN_xO_y.

In this article, we report the successful growth of high-quality epitaxial titanium oxynitrides with NaCl structure on MgO(001) substrates by pulsed laser deposition (PLD). The crystallinity, lattice parameter, microstructure, morphology, electrical, and mechanical properties of TiN_xO_y with different oxygen content were investigated. Defect analyses were also performed under various two-beam transmission electron microscopy (TEM) conditions.

2. Experimental

Titanium oxynitride films were grown in the PLD chamber with base pressure of 1×10^{-6} Torr. A 2-inch MgO(001) substrate was ultrasonically cleaned in acetone, then dried with nitrogen gas, and immediately loaded into the vacuum chamber. The substrate was placed opposite to a 2-inch oxygen-containing TiN target ($TiNO_{0.064}$) at a distance of 14 cm. The target was irradiated with a KrF (λ = 248 nm) laser beam at an angle of 45°, and rotated during deposition. Before

* Corresponding author. Tel.: +886 3 5731615; fax: +886 3 5724727.
E-mail address: dohienvl@gmail.com (H. Do).

0257-8972/$ – see front matter © 2012 Elsevier B.V. All rights reserved.
http://dx.doi.org/10.1016/j.surfcoat.2012.11.008

TiN_xO_y deposition, the MgO substrates were heat-treated at 700 °C for 30 min to obtain a smooth and clean surface. The deposition process was then carried out under several different conditions to obtain TiN_xO_y films with different oxygen content while the substrate temperature was fixed at 700 °C for all cases. After the deposition process had been completed, the substrate was cooled down to room temperature in 90 min. Chemical composition of the deposited films was determined by X-ray photoelectron spectroscopy (XPS) (ULVAC-PHI, PHI Quantera SXM) by using a monochromatic Al Kα radiation source. For the XPS quantitative analysis, the peak area was corrected with relative sensitivity factors from a manufacturer's program and database. A Bede D1 high-resolution X-ray diffractometer, equipped with a two-bounce Si 220 channel-cut collimator crystal, a dual channel Si 220 analyzer crystal, and $CuK\alpha_1$ radiation ($\lambda = 1.5406$ Å), was used to investigate the crystallinity and strain state of the films. Cross-sectional TEM specimens were prepared by tripod polishing method and focused ion beam (FIB) technique (FEI Nova 200). The tripod polished specimens were Ar-ion milled at angles of 4–6° and acceleration voltage of 4–5 kV. TEM specimens were then examined in a JEOL 2010F microscope. Atomic force microscopy (AFM) (D3100) was used to investigate the surface morphology of the films. Hall measurements were carried out to determine the resistivity and carrier concentration of the TiN_xO_y films.

The mechanical properties of the deposited TiN_xO_y films were characterized by using a MTS Nanoindenter XP system with a diamond Berkovich tip. The continuous-stiffness-measurement (CSM) mode was used with a harmonic force at 45 Hz imposed on the increasing load. To extract the accurate hardness and elastic modulus of the thin TiN_xO_y films on the MgO substrates, we applied the model developed by Han Li et al. [26], in which the substrate effect caused by elastic mismatch between the film and substrate was taken into account.

3. Results and discussion

The chemical composition of the deposited films was determined by XPS. Fig. 1 shows the XPS depth profiles of samples A and B with different oxygen content. As seen in Fig. 1, the chemical composition of both samples A and B is uniform and can be determined as $TiN_{0.97}O_{0.23}$ (sample A) and $TiN_{1.11}O_{0.10}$ (sample B), suggesting that the addition of oxygen atoms occurred in the overstoichiometric TiN_x ($x > 1$). The chemical states of both TiNO films were identified by examining Ti-2p, O-1s, and N-1s XPS spectra in high-resolution

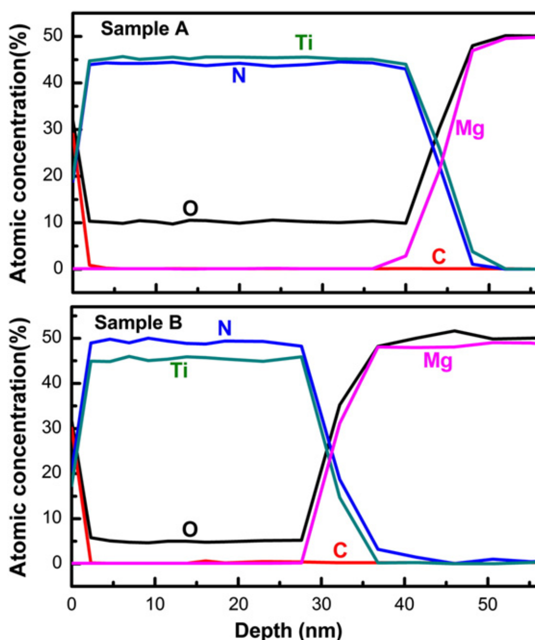

Fig. 1. XPS depth profiles for samples A and B with different oxygen content.

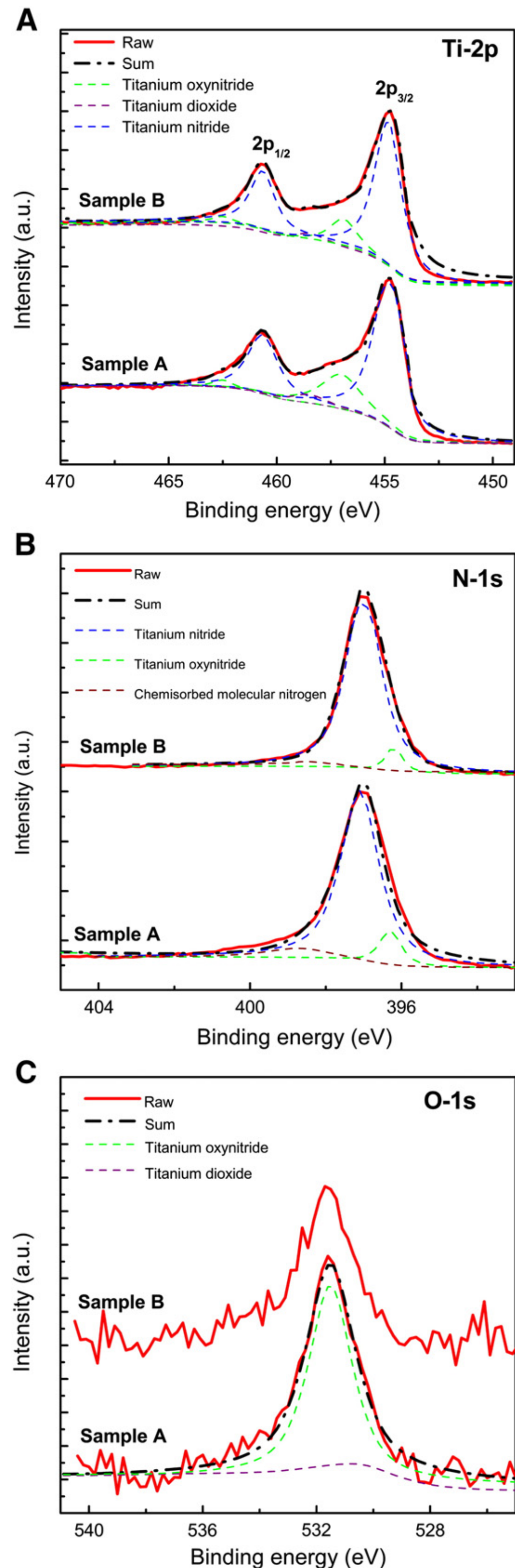

Fig. 2. XPS spectra for A) Ti-2p, B) N-1s, C) O-1s after Ar sputtering for one minute of samples A and B. The spectra are deconvoluted into components of titanium nitride, titanium oxynitride, and titanium dioxide [21,27,28].

mode after Ar sputtering for 1 min (~2 nm). As shown in Fig. 2A, the Ti-2p$_{3/2}$ peak of samples A and B can be deconvoluted into two main components of Ti–N bonding (454.9 eV corresponding to titanium nitride) and N–Ti–O bonding (~456.7 eV corresponding to titanium oxynitride) with a very small amount of Ti–O bonding (458.4 eV corresponding to titanium dioxide) [21,27,28]. The N-1s spectra for samples A and B (Fig. 2B) reveal a small amount of chemisorbed molecular nitrogen (398.7 eV) and two main components of titanium nitride (397 eV) and titanium oxynitride (396.2 eV) [27] in agreement with the results determined from the Ti peaks. In Fig. 2C, sample A shows a stronger O-1s signal compared with that of sample B due to the higher oxygen concentration incorporated into sample A.

The X-ray diffraction (XRD) patterns of both samples A and B in Fig. 3 show only $TiN_xO_y(002)$ and $TiN_xO_y(004)$ reflections in addition to the MgO ones, suggesting that (001) oriented single-phase titanium oxynitride have been deposited on MgO(001) substrates in our experimental conditions. Also, $TiN_xO_y(002)$ and $TiN_xO_y(004)$ reflections appear at 42.46° and 92.82° for sample A, and 42.41° and 92.63° for sample B, indicating that they have larger out-of-plane interplanar spacing than MgO. The X-ray rocking curves in the inset of Fig. 3 show that the full width at half maximum (FWHM) of $(002)TiN_xO_y$ is about 58 arcsec for sample A, and 64 arcsec for sample B, implying that both TiN_xO_y films deposited on MgO have a very good quality (the FWHM of the MgO substrate is 42 arcsec). The X-ray ϕ-scan was done on both films to verify the orientation relationship between the TiN_xO_y and MgO substrates. As seen in Fig. 4, four {022} peaks of MgO and TiNO appear at the same ϕ angles with a separation of 90°. This result suggests that the TiNO films have epitaxially grown on the MgO substrates with the cube-on-cube relationship of TiNO(001)//MgO(001) and TiNO[100]//MgO[100].

To investigate the effect of oxygen content on the strain state as well as the lattice parameters of TiN_xO_y films, XRD reciprocal space maps (RSM) of the asymmetric (113)MgO and $(113)TiN_xO_y$ reflections were acquired. As shown in Fig. 5, the asymmetric (113)MgO and TiN_xO_y reflections for both samples are almost vertically aligned, implying that TiN_xO_y lattices are in coherency with the MgO one. Hence, both TiN_xO_y films may be under fully compressive strain as a result from lattice mismatch and thermal mismatch with MgO. The thermal strain was induced due to a large difference in the coefficient of thermal expansion (CTE) of MgO and TiN_xO_y ($\alpha_{MgO}=13\times10^{-6}$ K^{-1} and assume $\alpha_{TiNO}\sim\alpha_{TiN}=9.35\times10^{-6}$ K^{-1} [29]). When substrate temperature dropped from 700 ° C down to room temperature, the

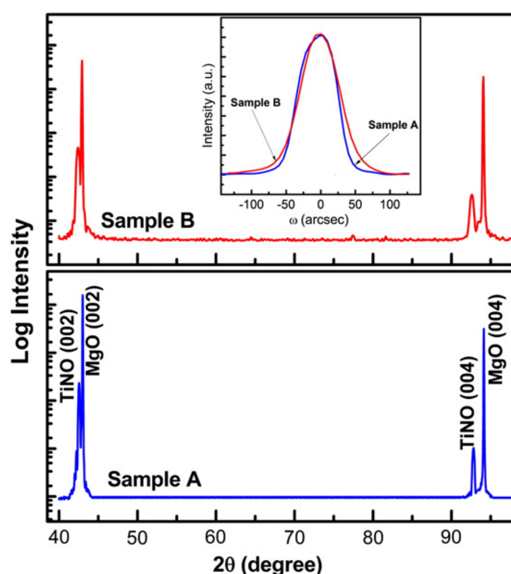

Fig. 3. XRD 2θ-θ scans for TiN_xO_y films. XRD ω-scan is shown in the inset.

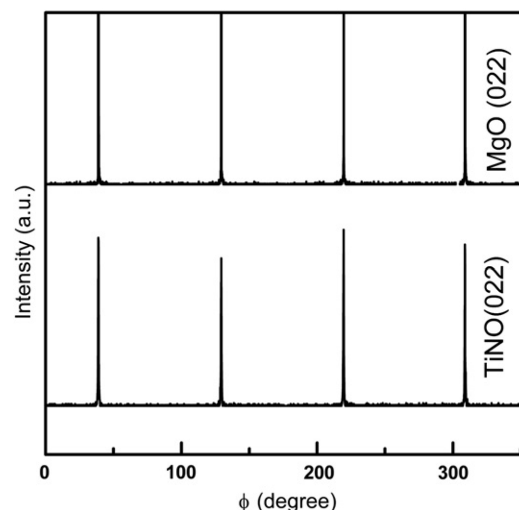

Fig. 4. XRD ϕ-scan of {022} reflections for TiN_xO_y film grown on the MgO substrate, showing epitaxial relationship between the film and the substrate is $TiN_xO_y(001)$//MgO(001) and $TiN_xO_y[100]$//MgO[100].

MgO substrate contracted more than the TiN_xO_y layer, resulting in the generation of a compressive strain of −0.27% in the TiN_xO_y layer. The out-of-plane, c, and in-plane, a, lattice parameters of TiNO can be determined as follows: $c=3/Q_z$, and $a=\sqrt{2}/Q_x$, where Q_z and Q_x are vertical and horizontal vectors that lie along MgO[001] and MgO[110] directions, respectively [29]. The relaxed lattice parameter a_o can be calculated from c and a by using equation: $a_o=c[1-2\nu(c-a)/c(1+\nu)]$ [29], where ν is the Poisson ratio of the deposited films. Due to the slight difference in the Poisson ratio between TiN and TiO ($\nu_{TiN}=0.22$ [29] and $\nu_{TiO}=0.232$ [30]) and the large ratio of N/O of the deposited TiNO films, we can assume that $\nu_{TiNO}\sim\nu_{TiN}$. By using MgO(113) peak as reference ($a_{MgO}=4.2112$ Å [29]), the lattice parameters (c, a, and a_o) and in-plane residual strain $\varepsilon_{||}$ of samples A and B can be calculated and are listed in Table 1. The results show that the lattice parameters of TiN_xO_y films decrease with the increase of oxygen concentration but still lie in the lattice parameter range between bulk TiN ($a_{TiN}=4.2417$ Å from the powder diffraction file PDF 38-1420) and bulk TiO ($a_{TiO}=4.1770$ Å, PDF 8-117). Those results are also in good agreement with the values reported in ref. [31]. Due to the fact that the radius of oxygen anion is smaller than that of the nitrogen anion, the substitution of oxygen for nitrogen enables the lattice parameter to decrease with increased oxygen concentration [32]. Additional to the effect of anion radii on the lattice parameter, the effect of electrostatic repulsion between N and O anions around Ti vacancies has also been taken into consideration [33]. Indeed, the XPS results above suggest that the substitution of oxygen for nitrogen occurs in the over-stoichiometric TiN_x, and such a non-stoichiometric structure has been reported to contain many Ti vacancies [34]. Therefore, there may have been an electrostatic repulsion between anions around Ti vacancies. Besides, the N atoms need three electrons to close its shell in order to achieve the most stable configuration (N^{-3}) while the O atoms only need two (O^{-2}) [33]. Hence, the replacement of N^{3-} by O^{-2} induces a decrease in the electrostatic repulsion between the anions around the Ti vacancies and consequently the lattice parameter decreases.

The second source of compressive strain can be generated from the film/substrate lattice mismatch that is determined as $\delta=[a_{MgO}-a_{film}]/a_{MgO}$. δ is −0.73% for pure TiN, −0.716% for sample B, and −0.655% for sample A. The result also shows that more oxygen content incorporated into the deposited films can reduce the lattice mismatch between MgO and TiN_xO_y. The corresponding critical thickness of samples A and B can be estimated theoretically as ~10 nm at room temperature. In other words, the addition of oxygen can result in the high-quality titanium

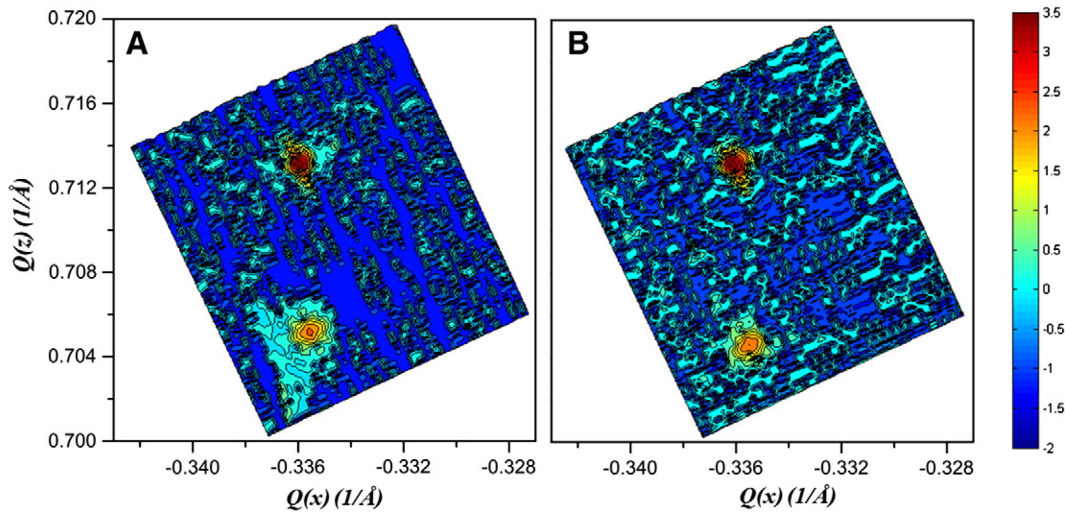

Fig. 5. Reciprocal space maps of the asymmetric (113)MgO and (113)TiN_xO_y reflections for A) sample A and B) sample B.

Table 1
In-plane *a*, out-of plane *c*, and relaxed a_o lattice parameters, and in-plane residual strain $\varepsilon_{||}$ of TiN_xO_y films.

Sample	a (Å)	c (Å)	a_o (Å)	$\varepsilon_{||}$ (%)
A ($TiN_{0.97}O_{0.23}$)	4.2116	4.2541	4.2388	−0.65
B ($TiN_{1.11}O_{0.10}$)	4.2124	4.2577	4.2414	−0.69

oxynitride with a composition which can make the deposited films to be excellently coherent with MgO, contrasting with the case of pure TiN on MgO. Indeed, the authors in ref. [29] have shown that the stoichiometric TiN film is semi-coherent with MgO that resulted from the generation of misfit dislocations at the TiN/MgO interface.

The surface morphology of the MgO substrates and the deposited films was examined by AFM. The film surface of samples A and B (Fig. 6) and the MgO substrate (not shown) is very uniform and smooth with root-mean-square roughness of 0.29 nm (sample A), 0.26 nm (sample B), and 0.18 nm (MgO).

The resistivity of TiN_xO_y films measured by the Hall measurement method was found to be 33 μΩ cm and 28 μΩ cm for samples A and B, respectively. In addition, the carrier concentration of samples A and B can be determined as high as 3.2×10^{22} cm^{-3} and 2.8×10^{22} cm^{-3}, indicating the metallic conduction behavior of the deposited films. The resistivity of the TiN_xO_y films are much smaller than that of the bulk TiO (190 μΩ cm) and about two times larger than that of the pure epitaxial TiN (~15 μΩ cm) [25]. It has been shown that the increasing resistivity in the series of TiN, TiN_xO_y, and TiO can be explained by considering the free electron concentration [35]. The lower free electron concentration results in poor conductivity of TiO and to a lesser extent TiN_xO_y [35]. The results can be compared with those reported in ref. [25], in which the resistivity of the epitaxial TiN_xO_y films, with oxygen concentration of 7.02–11.11 at.%, is about 21.0–32.3 μΩ cm [25]. Hence, compared with the polycrystalline TiNO films that have been shown to have the resistivity in the order of magnitude from mΩ cm to Ω cm [27,28] the epitaxial growth of the TiNO films certainly can greatly improve electrical conductivity.

The hardness (*H*) and Young's modulus (*E*) values are determined to be 23 ± 1.1 GPa and 400 ± 4.3 GPa for sample A, whereas sample B showed higher values of 26 ± 1.2 GPa and 430 ± 5.5 GPa, respectively. The results are closed with the reported values of stoichiometric TiN(001) with H~20 ± 0.8 GPa and E~445 ± 38 GPa [36]. It also clearly shows that both the hardness and elastic modulus of the TiN_xO_y films decrease as the amount of oxygen increases. The hardness and elastic modulus may also depend on the nitrogen content as they increase for the x in TiN_xO_y that increases from 0.97 to 1.11.

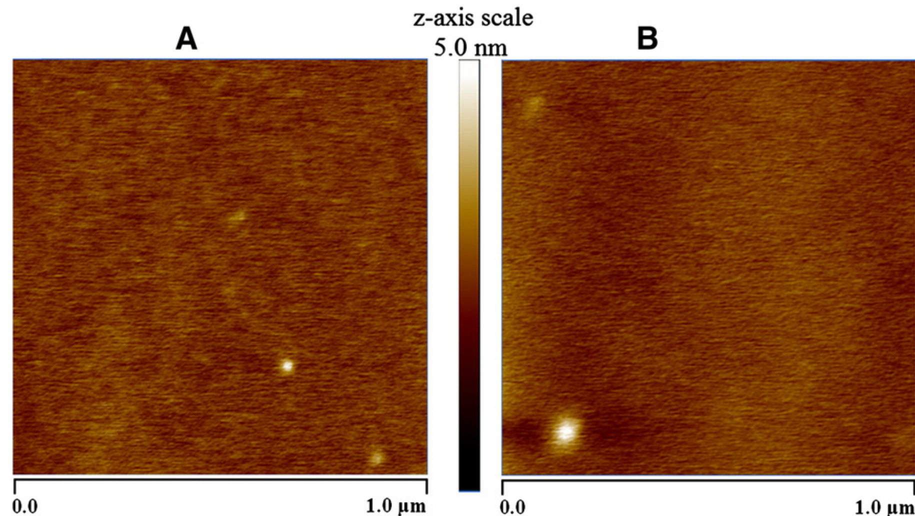

Fig. 6. AFM images of TiN_xO_y surface for A) sample A and B) sample B.

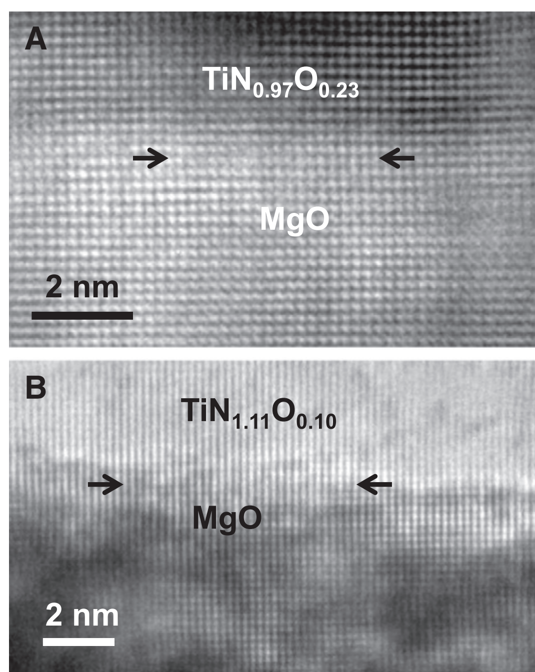

Fig. 7. Cross-sectional HRTEM images of A) sample A and B) sample B along [100] zone axis showing sharp and smooth interfaces between TiN_xO_y and MgO (indicated by arrows). No misfit dislocations at the interfaces can be observed over the range of 12–14 nm.

A similar evolution of *H* and *E* with oxygen content has also been reported for polycrystalline, textured, and bulk TiN_xO_y [7,33,37,38]. It could be due to that oxygen has a softening effect on those deposited films.

The epitaxial growth of TiNO on MgO is also confirmed by cross-sectional high-resolution TEM as shown in Fig. 7A and B for samples A and B along [100] zone axis. The high-resolution TEM images reveal sharp and smooth interfaces without any interlayer between the films and the substrates. No misfit dislocations at the coherent interface between TiN_xO_y and MgO in both samples can be identified in the range over 12–14 nm as a result of the very small in-plane lattice mismatch between them, consistent with the XRD data above.

Fig. 8A shows the cross-sectional bright field TEM image for sample B viewed along [100] zone axis. The corresponding selected area diffraction (SAD) pattern at the interface appears as a single-crystalline pattern, even though the RSM maps above show the MgO and TiNO reflections being separated from each other. This implies that TiNO has been epitaxially grown on MgO with the cube-on-cube relationship, but due to a very small lattice mismatch between TiNO and MgO, their diffraction spots cannot be distinguished due to the limit of the SAD resolution. To investigate the microstructural defects in the TiNO epilayers, the two-beam TEM technique was performed for sample B along [100] zone axis. As seen in Fig. 8B and C, cross-sectional bright-field TEM images obtained with different two-beam conditions of $\mathbf{g}=002$ and $\mathbf{g}=022$ show that no dislocations can be identified in the range of 250 nm. The dislocation density can be estimated from the XRD data [39,40] to be around $\sim 5\times 10^6$ cm^{-2}. Therefore, to identify one dislocation, the required observation range can be up to 10 μm that is far beyond the limited observation range in our specimens.

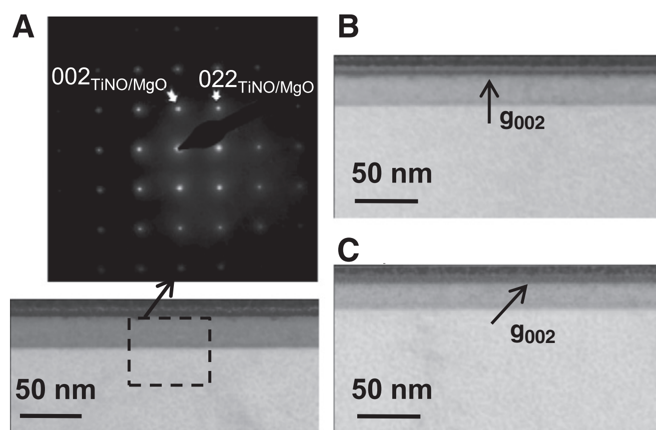

Fig. 8. A) Cross-sectional TEM image of sample B in [100] bright-field and the corresponding diffraction pattern at the film/substrate interface. Cross-sectional bright-field TEM images of sample B under two-beam condition of B) $\mathbf{g}=002$ and C) $\mathbf{g}=022$.

4. Conclusions

It has been illustrated that high-quality epitaxial TiN_xO_y films with a low density of defects have been grown successfully on MgO(001) substrates by pulsed laser deposition. The epitaxial relationship between the deposited films and substrates is TiNO(001)//MgO(001) and TiNO [100]//MgO[100]. The chemical composition of two epitaxial samples determined by XPS is $TiN_{0.97}O_{0.23}$ and $TiN_{1.11}O_{0.10}$ and the distribution is uniform throughout the film thickness. XRD and TEM show that both TiN_xO_y films have excellent coherency with MgO. It has also been demonstrated that the addition of oxygen reduces the lattice mismatch between TiN_xO_y and MgO. The surface of the deposited films is atomically smooth. The TiN_xO_y films are electrically conducting with the resistivity increasing with the oxygen content and decreasing with the nitrogen content. The oxygen-rich $TiN_{0.97}O_{0.23}$ film shows the hardness and Young's modulus values lower than those of the TiNO film enriched with nitrogen ($TiN_{1.11}O_{0.10}$).

Acknowledgments

The work was supported by National Science Council, Taiwan, ROC under Contract No. NSC 98-2221-E-009-042-MY3.

References

[1] H.O. Pierson, Handbook of Refractory Carbides and Nitrides: Properties, Characteristics, Processing and Applications, Noyes Publication, Westwood, New Jersey, USA, 1996.
[2] W.D. Sproul, R. Rothstein, Thin Solid Films 126 (1985) 257.
[3] S.R. Min, H.N. Cho, Y.L. Li, S.K. Lim, S.P. Choi, C.W. Chung, J. Ind. Eng. Chem. 14 (2008) 297.
[4] F. Fracassi, R. D'Agostino, R. Lamendola, I. Mangieri, J. Vac. Sci. Technol. A 13 (1995) 335.
[5] S. Benhenda, J.M. Guglielmacci, M. Gillet, L. Hultman, J.-E. Sundgren, Appl. Surf. Sci. 40 (1989) 121.
[6] S.P. Murarka, S.W. Hymes, CRC Crit. Rev. Solid State Mater. Sci. 20 (1995) 87.
[7] M. Braic, M. Balaceanu, A. Vladescu, A. Kiss, V. Braic, G. Epurescu, G. Dinescu, A. Moldovan, R. Birjega, M. Dinescu, Appl. Surf. Sci. 253 (2007) 8210.
[8] F. Vaz, P. Cerqueira, L. Rebouta, S.M.C. Nascimento, E. Alves, Ph. Goudeau, J.P. Rivière, Surf. Coat. Technol. 174 (2003) 197.
[9] M. Lazarov, P. Raths, H. Metzger, W. Spirkl, J. Appl. Phys. 77 (1995) 2133.
[10] Y. Saito, M. Hirata, H. Tada, M. Hyodo, Appl. Phys. Lett. 63 (1993) 1319.
[11] R. Asahi, T. Morikawa, T. Ohwaki, K. Aoki, Y. Taga, Science 293 (2001) 269.
[12] Y.X. Leng, P. Yang, J.Y. Chen, H. Sun, J. Wang, G.J. Wang, N. Huang, X.B. Tian, P.K. Chu, Surf. Coat. Technol. 138 (2001) 296.
[13] R.J. Koerner, L.A. Butterworth, I.V. Mayer, R. Dasbach, H.J. Busscher, Biomaterials 23 (2002) 2835.
[14] D.-H. Kang, D.-H. Ahn, M.-H. Kwon, H.-S. Kwon, K.-B. Kim, K.-S. Lee, B.-K. Cheong, Jpn. J. Appl. Phys. 43 (2004) 5243.
[15] X. Yang, C. Li, B. Yang, W. Wang, Y. Qian, Chem. Phys. Lett. 383 (2004) 502.
[16] P. Jin, S. Maruno, Jpn. J. Appl. Phys. 30 (1991) 2058.
[17] W. Ensinger, Nucl. Instrum. Methods Phys. Res., Sect. B 56 (1991) 648.
[18] N. Kumar, M.G. Fissel, K. Pourrezaei, B. Lee, E.C. Douglas, Thin Solid Films 153 (1987) 287.
[19] W. Sinke, G.P.A. Frijlink, F.W. Saris, Appl. Phys. Lett. 47 (1985) 471.
[20] N. Kumar, J.T. McGinn, K. Pourrezaei, B. Lee, E.C. Douglas, J. Vac. Sci. Technol. A 6 (1986) 1602.

[21] J. Graciani, J.F. Sanz, T. Asaki, K. Nakamura, J.A. Rodríguez, J. Chem. Phys. 126 (2007) 244713.
[22] O. Diwald, T.L. Thompson, T. Zubkov, Ed.G. Goralski, S.D. Walck, J.T. Yates, J. Phys. Chem. B 108 (2004) 6004.
[23] F. Mauri, F.-D. Duminica, Surf. Coat. Technol. 205 (2010) 1287.
[24] Y. Suda, H. Kawasaki, T. Ueda, T. Ohshima, Thin Solid Films 453 (2004) 162.
[25] R. Chowdhury, R.D. Vispute, K. Jagannadham, J. Narayan, J. Mater. Res. 11 (1996) 1458.
[26] H. Li, J.J. Vlassak, J. Mater. Res. 24 (2009) 1114.
[27] A. Trenczek-Zajac, M. Radecka, K. Zakrzewska, A. Brudnik, E. Kusior, S. Bourgeois, M.C. Marco de Lucas, L. Imhoff, J. Power Sources 194 (2009) 93.
[28] M.-H. Chan, F.-H. Lu, Surf. Coat. Technol. 203 (2008) 614.
[29] C.-S. Shin, D. Gall, N. Hellgren, J. Patscheider, I. Petrov, J.E. Greene, J. Appl. Phys. 93 (2003) 6025.
[30] Y.O. Ciftci, Y. Ünlü, K. Colakoglu, E. Deligoz, Phys. Scr. 80 (2009) 025601.
[31] M. Radecka, E. Pamula, A. Trenczek-Zajac, K. Zakrzewska, A. Brudnik, E. Kusior, N.T.H. Kim-Ngan, A.G. Balogh, Solid State Ionics 192 (2011) 693.
[32] P. Jin, S. Maruno, Jpn. J. Appl. Phys. 30 (1991) 2058.
[33] J. Graciani, S. Hamad, J.F. Sanz, Phys. Rev. B 80 (2009) 184112.
[34] P. Patsalas, S. Logothetidis, J. Appl. Phys. 90 (2001) 4725.
[35] E. Vogelzang, J. Sjoeema, H. Boer, J. De Hosson, J. Appl. Phys. 61 (1987) 4606.
[36] H. Ljungcrantz, M. Odén, L. Hultman, J.E. Greene, J.-E. Sundgren, J. Appl. Phys. 80 (1996) 6725.
[37] J.-M. Chappe, N. Martin, J. Lintymer, F. Sthal, G. Terwagne, J. Takadoum, Appl. Surf. Sci. 253 (2007) 5312.
[38] F. Vaz, P. Cerqueira, L. Rebouta, S.M.C. Nascimento, E. Alves, Ph. Goudeau, J.P. Rivière, K. Pischow, J. de Rijk, Thin Solid Films 447 (2004) 449.
[39] P. Gay, P.B. Hirsch, A. Kelly, Acta Metall. 1 (1953) 315.
[40] C. Dunn, E. Koch, Acta Metall. 1 (1957) 548.